Photoplethysmography-Based Algorithm for Detection of Cardiogenic Output During Cardiopulmonary Resuscitation

Ralph W. C. G. R. Wijshoff*, Antoine M. T. M. van Asten, Wouter H. Peeters, Rick Bezemer, Gerrit Jan Noordergraaf, Massimo Mischi, *Senior Member, IEEE*, and Ronald M. Aarts, *Fellow, IEEE*

***Abstract*—Detecting return of spontaneous circulation (ROSC) during cardiopulmonary resuscitation (CPR) is challenging, time consuming, and requires interrupting chest compressions. Based on automated-CPR porcine data, we have developed an algorithm to support ROSC detection, which detects cardiogenic output during chest compressions via a photoplethysmography (PPG) signal. The algorithm can detect palpable and impalpable spontaneous pulses. A compression-free PPG signal which estimates the spontaneous pulse waveform, was obtained by subtracting the compression component, modeled by a harmonic series. The fundamental frequency of this series was the compression rate derived from the transthoracic impedance signal measured between the defibrillation pads. The amplitudes of the harmonic components were obtained via a least mean-square algorithm. The frequency spectrum of the compression-free PPG signal was estimated via an autoregressive model, and the relationship between the spectral peaks was analyzed to identify the pulse rate (PR). Resumed cardiogenic output could also be detected from a decrease in the baseline of the PPG signal, presumably caused by a redistribution of blood volume to the periphery. The algorithm indicated cardiogenic output when a PR or a redistribution of blood volume was detected. The algorithm indicated cardiogenic output with 94% specificity and 69% sensitivity compared to the retrospective ROSC detection of nine clinicians. Results showed that ROSC detection can be supported by combining the compression-free PPG signal with an indicator based on the detected PR and redistribution of blood volume.**

***Index Terms*—Autoregressive (AR) model, cardiogenic output, cardiopulmonary resuscitation (CPR), harmonic model, least mean-square (LMS), photoplethysmography (PPG), pulse rate (PR), return of spontaneous circulation (ROSC), spectral analysis, spontaneous pulse, transthoracic impedance (TTI).**

Manuscript received August 1, 2014; revised October 16, 2014; accepted November 7, 2014. Date of publication November 13, 2014; date of current version February 16, 2015. This work was supported by NL Agency, IOP Photonic Devices, IPD083359 HIP Hemodynamics by Interferometric Photonics. *Asterisk indicates corresponding author*.

*R. W. C. G. R. Wijshoff is with the Department of Electrical Engineering, Eindhoven University of Technology, Eindhoven, The Netherlands, and also with Philips Research, Eindhoven, The Netherlands (e-mail: ralph.wijshoff@philips.com).

A. M. T. M. van Asten, W. H. Peeters, and R. Bezemer are with Philips Research, Eindhoven, The Netherlands.

G. J. Noordergraaf is with the Department of Anaesthesiology and Resuscitation and the CPRLab, St. Elisabeth Hospital, Tilburg, The Netherlands.

M. Mischi is with the Department of Electrical Engineering, Eindhoven University of Technology, Eindhoven, The Netherlands.

R. M. Aarts is with the Department of Electrical Engineering, Eindhoven University of Technology, and also with Philips Research, Eindhoven, The Netherlands.

Color versions of one or more of the figures in this paper are available online at http://ieeexplore.ieee.org.

Digital Object Identifier 10.1109/TBME.2014.2370649

I. Introduction

HIGH-QUALITY cardiopulmonary resuscitation (CPR) requires minimizing interruptions of chest compressions, as interruptions reduce blood flow and, thus, the chance of achieving return of spontaneous circulation (ROSC) [1]–[5]. International guidelines state that interruptions for ROSC assessment should last at most 10 s [2], [3]. ROSC is assessed by analyzing the electrocardiographic rhythm and checking for a palpable circulatory pulse. In practice, however, pulse checks by manual palpation can take significantly longer than 10 s, especially when a spontaneous pulse is absent [6], [7]. Furthermore, the interpretation of manual palpation is known to be unreliable, even when performed by expert clinicians [6], [7]. Therefore, an objective method to detect presence or absence of a spontaneous pulse, especially during compressions, would be valuable to support ROSC detection.

Monitoring end-tidal CO_2 [8], [9], invasive blood pressure [10], [11], or central venous oxygen saturation [12] allows for a more objective assessment of ROSC, also during compressions, but requires a secured airway or placement of catheters. Transthoracic impedance (TTI) measurements [13]–[15] and near-infrared spectroscopy (NIRS) [16], [17] are noninvasive methods, but TTI is strongly influenced by compressions and NIRS responds slowly upon ROSC. Generally, photoplethysmography (PPG) is an easy to use and noninvasive technique to continuously measure a spontaneous pulse [18], [19]. Its potential to measure a spontaneous pulse during compressions has been observed in an automated-CPR animal study [20]. When the complexity of the PPG signal increased during compressions, the invasive blood pressure indicated presence of a spontaneous pulse. Furthermore, frequency spectra of the PPG signals showed that the spontaneous pulse rate (PR) and compression rate could be distinguished. Although these methods can provide valuable support, ROSC detection remains a clinical situational assessment, because it involves determining whether a perfusing rhythm is life sustaining.

This paper describes a PPG-based algorithm that detects cardiogenic output during chest compressions to support ROSC detection, developed based on preclinical data from [20]. Cardiogenic output was detected using the compression-free PPG signal and the baseline of the PPG signal. The compression-free PPG signal was obtained by subtracting the compression component from the PPG signal, to estimate the spontaneous pulse waveform. We defined a spontaneous pulse in the PPG

signal as a (quasi-)periodic feature resulting from cardiac contractions. The spontaneous pulse can be palpable or impalpable. The compression component subtracted from the PPG signal was determined via a harmonic series. The fundamental frequency of this series was the compression rate derived from the TTI signal. The TTI signal had been measured between the defibrillation pads, as is common in defibrillators. The frequency spectrum of the compression-free PPG signal was analyzed to detect the PR. When cardiogenic output resumed, the baseline of the PPG signal decreased, presumably caused by a redistribution of blood volume to the periphery. The algorithm indicated cardiogenic output when a PR or a decrease in the baseline of the PPG signal was detected.

II. Methods

A. Experimental Measurements

An automated-CPR study was conducted on 16 pigs [20]. All animals received care compliant with the Dutch Animal Experimentation Law and the Standard Operation Procedures of the Central Animal Laboratory of the Radboud University Nijmegen Medical Center, where the experiments were conducted. The Radboud University Animal Ethical Committee approved the protocol. The experiments, protocol, and physiological data are described in detail in [20].

After a 10-min baseline recording, cardiac arrest was induced via an electrical shock, followed by 20 min of CPR in a rhythm of 30 compressions alternated by two ventilations (30:2 rhythm). Chest compressions were delivered by an automated CPR device at a rate of 100 min^{-1}. After 20 min of CPR, 2-min cycles were initiated to achieve ROSC, each starting with defibrillation if appropriate, followed by 30:2 CPR. If ROSC was achieved after one of the cycles, CPR stopped and measurements continued for 20-min post-ROSC. Otherwise the experiment ended after the fourth cycle. Animals were euthanized at the end of the experiment.

All animals were monitored by electrocardiography (ECG), capnography, and pulse oximetry, and by measuring arterial blood pressure (ABP) in the aortic arch, and carotid artery blood flow. Near-infrared (900 nm) PPG signals [Volt] were obtained using a forehead reflectance pulse oximetry probe (Nellcor Oxisensor II RS-10, Covidien-Nellcor, Dublin, Ireland), controlled by a custom-built photoplethysmograph. The probe was customized to enable placement by suturing between the nostrils, because this site is relatively stable in terms of motion, and allows for tight fixation of the probe to the skin. TTI [Ohm] between Adult Plus Multifunction Electrode Pads M3713A (Philips, Andover, MA, USA) was recorded via the HeartStart MRx Monitor/Defibrillator (Philips, Andover, MA, USA).

PPG and ABP waveforms were recorded simultaneously using a 16-bit digital data acquisition card (DAQ) (NI USB-6259, National Instruments, Austin, TX, USA). The DAQ was controlled by dedicated software implemented in LabVIEW (National Instruments, Austin, TX, USA).

All waveforms were sampled at $f_s = 250$ Hz. The TTI signal was synchronized to the PPG signal by resampling and translating the TTI signal such that correlation was maximal between the fundamental compression frequency components in the TTI and ABP signals. Resampling was done at rates between 249.91 and 250.09 Hz in steps of 0.01 Hz.

B. Overview of the Algorithm

Fig. 1 outlines the algorithm that indicated cardiogenic output during CPR. The algorithm contained three modules: one for removal of the compression component and PR detection (purple and green blocks in Fig. 1, Sections II-C–II-F), one for analysis of the PPG signal baseline (yellow blocks in Fig. 1, Section II-G), and one for the indicator of cardiogenic output (blue blocks in Fig. 1, Sections II-H and II-I).

The primary input of the algorithm was the raw PPG signal $\text{ppg}[n]$, with sample index n. A band-pass filtered PPG signal $\text{ppg}_{\text{ac}}[n]$ was obtained via a first-order Butterworth low-pass filter with a 12 Hz cutoff and a fourth-order Butterworth high-pass filter with an 0.3 Hz cutoff. By using the compression rate derived from the auxiliary TTI signal $Z[n]$ (see Section II-C), the compression component was removed from $\text{ppg}_{\text{ac}}[n]$ to obtain the compression-free PPG signal $\text{ppg}_{\text{cf}}[n]$ (see Section II-D). The frequency spectrum of $\text{ppg}_{\text{cf}}[n]$ was determined via an autoregressive (AR) model (see Section II-E). The PR was identified in the spectrum, if it contained a signal with sufficient high-frequency content (see Section II-F). In parallel, the baseline of the PPG signal $\text{ppg}_{\text{bl\_d}}[n]$ was obtained by low-pass filtering at 0.5 Hz. A presumable redistribution of blood volume to the periphery could be detected from a decrease in $\text{ppg}_{\text{bl\_d}}[n]$ (see Section II-G). The algorithm indicated cardiogenic output when a PR or a decrease in the baseline was detected (see Sections II-H and II-I). In this study, we have not extensively optimized the algorithm parameter values, because of the small preclinical dataset.

C. Determination of Compression Characteristics

The instantaneous compression frequency and phase were determined from the TTI signal, for which it has been used before [21], [22]. To extract the fundamental compression frequency component, the TTI signal $Z[n]$ was band-limited by a fourth-order Butterworth filter with a pass-band between 1 and 3 Hz. This accommodates the range of manual chest compression frequencies between about 60 and 180 min^{-1} observed in clinical practice [21]–[23].

The band-limited TTI signal, indicated by $Z_f[n]$, had a sinusoidal-like shape, with local minima occurring at the end of a compression. Compressions were detected by finding consecutive sequences of a local maximum $(n_l, Z_{f\max l})$, a local minimum $(n_c, Z_{f\min c})$, and a local maximum $(n_r, Z_{f\max r})$. The local extremes were found from the zero crossings in the time derivative of $Z_f[n]$. It was required that $Z_{f\max l,r} \geq 0$ and $Z_{f\min c} < 0$. To avoid detecting ventilations, motion artifacts, or noise, a sequence of three local extremes had to meet four criteria to be associated with a compression:

1) The amplitude was within a specified range:

$$Z_{lb} \leq \frac{Z_{f\max l} + Z_{f\max r}}{2} - Z_{f\min c} \leq Z_{ub}, \quad (1)$$

with limits $Z_{lb} = 0.2\ \Omega$ and $Z_{ub} = 10\ \Omega$ [15].

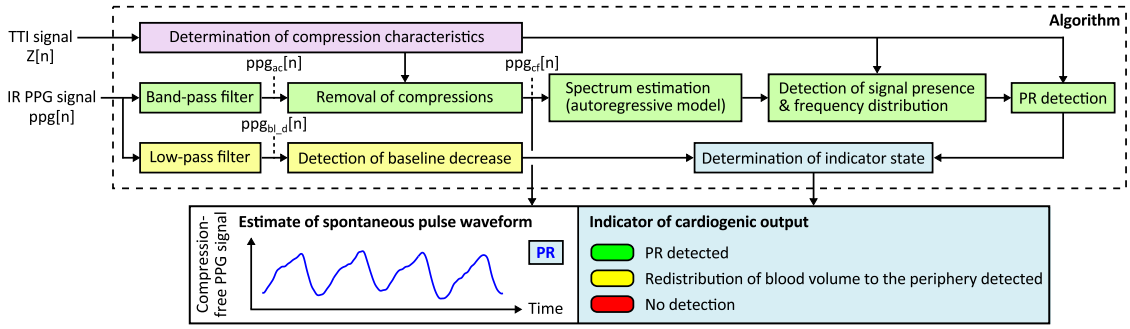

Fig. 1. Overview of the PPG-based algorithm that indicated cardiogenic output during CPR. A compression-free IR PPG signal, $\mathrm{ppg_{cf}}[n]$, containing an estimate of the spontaneous pulse waveform, was obtained by removing the compression component. The compression removal stage used the compression rate determined from the auxiliary TTI signal $Z[n]$. The frequency spectrum of $\mathrm{ppg_{cf}}[n]$ was estimated via an AR model. The PR was determined in this spectrum, if it contained a signal with sufficient high-frequency content. A presumable redistribution of blood volume to the periphery was detected from a decrease in the baseline of the IR PPG signal $\mathrm{ppg_{bl\_d}}[n]$. Cardiogenic output was indicated if a PR or a decrease in baseline was detected. AR: autoregressive; CPR: cardiopulmonary resuscitation; IR: infrared; PPG: photoplethysmography; PR: pulse rate; TTI: transthoracic impedance.

2) The distance $n_r - n_l$ was within a specified range:

$$n_{lb} \leq n_r - n_l \leq n_{ub}, \tag{2}$$

with initially $n_{lb} = n_{lb0} = 0.3\,\mathrm{s} \cdot f_s$ and $n_{ub} = n_{ub0} = 1\,\mathrm{s} \cdot f_s$ to allow for compression rates of 60–200 min^{-1}. After detection of at least N_D compressions, the bounds changed to $n_{lb,i} = (1 - k_D)n_{D,i}$ and $n_{ub,i} = (1 + k_D)n_{D,i}$, with $0 < k_D < 1$ setting the allowed deviation from $n_{D,i} = N_D^{-1} \sum_{i'=i-N_D+1}^{i} (n_{r,i'} - n_{l,i'})$, with i indicating the most recently detected compression. If $n_{lb,i}$ or $n_{ub,i}$ became incompliant with compression rates of 60–200 min^{-1}, or if N_D sequential sequences failed this criterion, the bounds were reset to n_{lb0} and n_{ub0}.

3) The sequence was sufficiently symmetric in time:

$$\frac{1}{k_T} \leq \frac{n_c - n_l}{n_r - n_c} \leq k_T, \tag{3}$$

where parameter $k_T > 1$ set the allowed asymmetry.

4) The sequence was sufficiently symmetric in amplitude:

$$\frac{1}{k_A} \leq \frac{-Z_{f\min c}}{(Z_{f\max l} + Z_{f\max r})/2} \leq k_A, \tag{4}$$

where parameter $k_A > 1$ set the allowed asymmetry. This criterion was only met if $Z_{f\max l} + Z_{f\max r} > 0$.

After identifying the individual compressions, first the instantaneous chest compression frequency $f_{cc,i}$ associated with compression i was determined from the distance between two consecutive local minima. If they were at most 1 s apart,

$$f_{cc,i} = \frac{f_s}{n_{c,i} - n_{c,i-1}}. \tag{5}$$

If a local minimum was not preceded by another local minimum within 1 s, a new sequence of chest compressions was assumed to have started. In that case, the compression frequency associated with the second compression of the sequence was also associated with the first compression of the sequence. This implies an inherent delay in the algorithm of at least two compressions. Compressions more than 1 s apart from both neighboring compressions were ignored.

Second, the onset $n_{o,i}$ of compression i was determined as

$$n_{o,i} = n_{c,i} - \frac{f_s}{f_{cc,i}}. \tag{6}$$

Third, by starting at the onset of compression i, the compression phase $\phi_{cc}[n]$ [rad] was determined as

$$\phi_{cc}[n] = \phi_{cc}[n-1] + 2\pi \frac{f_{cc,i}}{f_s}, \quad n_{o,i} \leq n < n_{o,i+1}. \tag{7}$$

Compression phase $\phi_{cc}[n]$ was initialized at 0 rad, and was reset to 0 rad, when a new compression sequence started.

Fourth, a smooth envelope function $A[n]$ [-] was constructed, indicating presence of compressions. $A[n]$ equaled 1 during a compression that was not the first of a sequence. For the first compression of a sequence, $A[n]$ smoothly increased from 0 to 1 in $N_{o,i} = \mathrm{round}\,(f_s/(4f_{cc,i}))$ samples via

$$\frac{1}{2}\left(1 - \cos\left(\pi \frac{n - n_{o,i}}{N_{o,i}}\right)\right), \quad n_{o,i} \leq n \leq n_{o,i} + N_{o,i}, \tag{8}$$

after which $A[n]$ equaled 1 during the remaining compression period. After the last compression of a sequence, $A[n]$ smoothly decreased from 1 to 0 in $N_{o,i}$ samples via

$$\frac{1}{2}\left(1 + \cos\left(\pi \frac{n - n_{c,i}}{N_{o,i}}\right)\right), \quad n_{c,i} \leq n \leq n_{c,i} + N_{o,i}. \tag{9}$$

Otherwise $A[n]$ equaled 0.

Based on the measured TTI signals, $N_D = 5$, $k_D = 0.35$, and $k_T = k_A = 3$ were used for all animals.

D. Removal of the Compression Component

To estimate the spontaneous pulse waveform, that can support the clinician in detecting ROSC, a harmonic series was employed to model and remove the chest compression component in the PPG signal. A harmonic series has been employed successfully before to model and remove the chest compression component in the ECG signal [21], [23], [24].

The primary input of the compression removal stage was the band-pass filtered PPG signal $\mathrm{ppg_{ac}}[n]$, that we assumed to be a sum of a spontaneous pulse component $\mathrm{sp}[n]$, a compression

component cmp$[n]$, and remaining components r$[n]$ [20]:

$$\text{ppg}_{ac}[n] = \text{sp}[n] + \text{cmp}[n] + \text{r}[n]. \tag{10}$$

Here, r$[n]$ contains noise and possibly frequency components resulting from interaction between spontaneous cardiac activity and compressions [20]. Interaction frequencies were observed at the sum and the difference of the compression rate and the PR and their harmonics [20]. A compression-free PPG signal $\text{ppg}_{\text{cf}}[n]$, containing an estimate of the spontaneous pulse component, was obtained by subtracting the estimate of the compression component, $\text{cmp}_{est}[n]$:

$$\text{ppg}_{cf}[n] = \text{ppg}_{\text{ac}}[n] - \text{cmp}_{est}[n]. \tag{11}$$

The estimate $\text{cmp}_{est}[n]$ was modeled by a harmonic series of K in-phase and quadrature terms with fundamental frequency $f_{cc,i}$ determined from the TTI signal [23], [24]:

$$\begin{aligned}\text{cmp}_{est}[n] = \; & A[n]\sum_{k=1}^{K}\left[a_k[n]\cos\left(k\phi_{cc}[n]\right)\right. \\ & \left.+b_k[n]\sin\left(k\phi_{cc}[n]\right)\right], \end{aligned}\tag{12}$$

with envelope function $A[n]$ (see Section II-C), compression phase $\phi_{cc}[n]$ (7), and $a_k[n]$ and $b_k[n]$ [Volt] the amplitudes of the in-phase and quadrature terms of the kth harmonic, respectively. $A[n]$ quickly forced $\text{cmp}_{est}[n]$ to 0 during interruptions of compressions, so that input $\text{ppg}_{\text{ac}}[n]$ stayed unaffected in these interruptions. Amplitudes $a_k[n]$ and $b_k[n]$ were estimated via a least mean-square (LMS) algorithm [24]–[26]:

$$a_k[n+1] = a_k[n] + 2\mu A[n]\text{ppg}_{cf}[n]\cos\left(k\phi_{cc}[n]\right), \tag{13}$$

$$b_k[n+1] = b_k[n] + 2\mu A[n]\text{ppg}_{cf}[n]\sin\left(k\phi_{cc}[n]\right), \tag{14}$$

for $k = 1, \ldots, K$, and with step-size parameter μ.

The transfer function of the LMS filter between $\text{ppg}_{\text{ac}}[n]$ and $\text{ppg}_{\text{cf}}[n]$ can be approximated by a cascade of K notch filters having the notch centered at $kf_{cc}, k = 1, \ldots, K$, when the estimate of the compression frequency is stable at f_{cc}, $A[n] = 1$, and the step-size parameter $\mu < 1$ [25], [26]:

$$H(z) \approx \prod_{k=1}^{K}\frac{z^2 - 2z\cos\left(2\pi\frac{kf_{cc}}{f_s}\right) + 1}{z^2 - 2(1-\mu)z\cos\left(2\pi\frac{kf_{cc}}{f_s}\right) + (1-2\mu)}. \tag{15}$$

Each notch has a 3-dB bandwidth W [Hz] of about [24], [25]

$$W \approx \frac{\mu f_s}{\pi}. \tag{16}$$

Furthermore, μ determined the convergence time T_{cv} [s] to a fraction $0 < v < 1$ of the targeted values for a_k and b_k via

$$T_{cv} = \frac{1}{f_s}\frac{\ln(1-v)}{\ln(1-\mu)}. \tag{17}$$

We used $K = 9$ to remove all compression harmonics from $\text{ppg}_{\text{ac}}[n]$ which remained in the frequency band that was to be analyzed for PR detection. High harmonics could result from probe motion relative to the skin. To limit the removal of PRs to ranges of about 95–105 min^{-1} and 195–205 min^{-1}, we set $\mu = 0.002$, resulting in $W \approx 10$ min^{-1}, and $T_{c0.95} \approx 6$ s.

E. Spectrum Estimation

1) AR Model: Frequency spectra of the compression-free PPG signal $\text{ppg}_{\text{cf}}[n]$ were determined over time via AR models. Because $\text{ppg}_{\text{cf}}[n]$ was nonstationary, spectra could only be estimated from short time windows. AR models provide a better frequency resolution on short time windows compared to the Fast Fourier Transform [27]–[29].

Prior to determining the AR models, $\text{ppg}_{\text{cf}}[n]$ was downsampled to $f_{s\_d} = 31.25$ Hz. Downsampling increases the phase angle of the poles in the data, resulting in more reliable estimation of the AR coefficients [30]. Downsampling was done in three consecutive steps to avoid numerical issues. First, a third-order Butterworth low-pass filter with a 12 Hz cutoff was applied, followed by downsampling to 125 Hz. Second, a sixth-order Butterworth low-pass filter with a 12 Hz cutoff was applied, followed by downsampling to 62.5 Hz. Third, a sixth-order Butterworth low-pass filter with a 12 Hz cutoff was applied, followed by downsampling to $f_{s\_d} = 31.25$ Hz.

The AR models were then estimated from the downsampled compression-free PPG signal $\text{ppg}_{\text{cf\_d}}[n]$ [27]:

$$\text{ppg}_{cf\_d}[n] = -\sum_{p=1}^{P}\alpha_p\text{ppg}_{cf\_d}[n-p] + e[n], \tag{18}$$

with AR coefficients α_p, model order P, and prediction error $e[n]$. If P is sufficiently large, all correlations in the data are described by the linear prediction in (18) and the prediction error $e[n]$ is white noise [27]. For each AR model, the power spectral density (PSD) is obtained as a continuous function of frequency f [27]:

$$P_{\text{AR}}(f) = \frac{\sigma_e^2/f_{s\_d}}{\left|1 + \sum_{p=1}^{P}\alpha_p\exp\left(-j2\pi pf/f_{s\_d}\right)\right|^2}, \tag{19}$$

with prediction error power σ_e^2. The AR coefficients α_p were obtained from time windows of $T_w = 5$ s using the forward–backward approach [27]. The AR coefficients were computed once per second by translating these windows by 1 s. $P_{\text{AR}}(f)$ was evaluated on a 1 min^{-1} resolution.

2) Model Order: The AR model order P should be sufficient to capture the strongest frequency components present in $\text{ppg}_{\text{cf\_d}}[n]$. P was determined empirically using the prediction error. As a function of model order, the prediction error power was determined relative to the total signal power in the window from which the AR model was estimated. P was selected as the smallest order with the mean plus two standard deviations of the relative prediction error power at most 5%.

Model orders between 2 and 50 with increments of two were considered. AR models were estimated from $T_w = 5$ s sliding windows, with 4-s overlap. For all animals with ROSC, AR models were estimated in the 2-min cycle between successful defibrillation and the end of CPR. Therefore, for each model order the relative prediction error power was determined for 115 AR models. In [31], Ulrych and Ooe suggest that satisfactory results are often obtained if the model order does not exceed $1/3$ to $1/2$ of the available data points. This criterion was met by

considering model orders of at most 50 for $T_w = 5$ s windows at a sampling rate of $f_{s\_d} = 31.25$ Hz.

F. Spectral Analysis

If a signal with sufficient high-frequency content was detected in $\mathrm{ppg}_{\mathrm{cf\_d}}[n]$ (see Section II-F1), an iterative algorithm identified the PR among the peaks in $P_{\mathrm{AR}}(f)$ (see Section II-F2). The PR detection was evaluated via the ABP (see Section II-F3).

1) Signal Presence: To detect presence of a potential spontaneous pulse in compression-free PPG signal $\mathrm{ppg}_{\mathrm{cf\_d}}[n]$, we defined two criteria. One criterion required the prediction error power $P_e[n]$ to be smaller than a fraction $R_P \ll 1$ of the total signal power $P_s[n]$. The other criterion required the power of the low frequencies to be smaller than a fraction $R_D < 1$ of the total signal power. Both criteria were evaluated in each window from which the AR model in (18) had been determined. Specifically, we considered a signal present if

$$\frac{P_e[n]}{P_s[n]} < R_P, \tag{20}$$

and if

$$\frac{\sum_{0 \le f' < f_l} P_{AR}(f')}{\sum_{0 \le f' \le f_{s\_d}/2} P_{AR}(f')} < R_D, \tag{21}$$

with $f_l = 40$ min^{-1} the lower PR limit, below the bradycardia limit at 50 min^{-1} [2], and considered a minimum rate predictive of a potential ROSC [9]. If (20) or (21) did not hold, no signal was considered present. If both held, the peaks in $P_{\mathrm{AR}}(f)$ were analyzed to identify the PR.

In (20), the prediction error power was computed as

$$P_e[n] = \frac{1}{N_w - P} \sum_{i=n-N_w+1+P}^{n} \mathrm{e}^2[i], \tag{22}$$

and the total signal power was computed as

$$P_s[n] = \frac{1}{N_w - P} \sum_{i=n-N_w+1+P}^{n} \mathrm{ppg}^2_{cf\_d}[i], \tag{23}$$

with AR model order P and window length $N_w = \lceil T_w \cdot f_{s\_d} \rceil$. The first P samples were omitted, as there is no prediction.

If (20) held, $\mathrm{ppg}_{\mathrm{cf\_d}}[n]$ contained periodic components. In that case, correlations in the signal resulted in a large contribution of the linear prediction in (18) to $\mathrm{ppg}_{\mathrm{cf\_d}}[n]$, causing the prediction error power to be much smaller than the total signal power. If periodic components were absent, $\mathrm{ppg}_{\mathrm{cf\_d}}[n]$ mainly contained noise, resulting in a smaller contribution of the linear prediction to $\mathrm{ppg}_{\mathrm{cf\_d}}[n]$, and a larger ratio between prediction error power and total signal power.

Low-frequency oscillations could cause (20) to hold, whereas $\mathrm{ppg}_{\mathrm{cf\_d}}[n]$ contained no frequencies potentially corresponding to a PR. Such low-frequency oscillations occurred during compressions or interruptions of compressions. Therefore, (21) required a limited contribution of low frequencies to the signal power, to ascertain that $\mathrm{ppg}_{\mathrm{cf\_d}}[n]$ contained frequencies potentially corresponding to a PR. Equation (21) was only considered, if the TTI signal contained compressions in the window from which the AR model had been estimated.

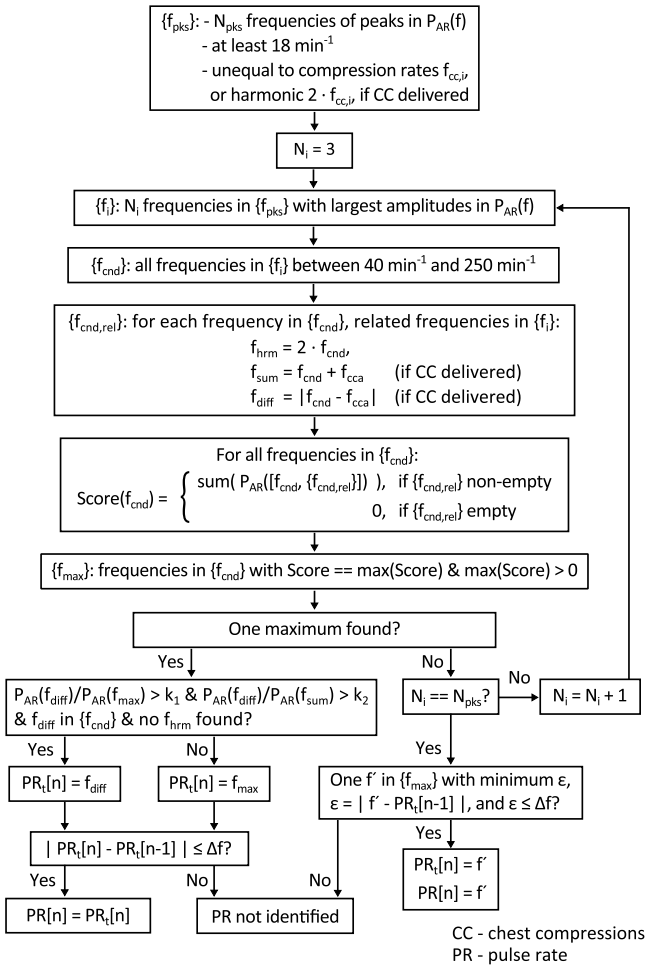

Fig. 2. Flowchart of the iterative algorithm that identified the PR among the peaks in PSD $P_{\mathrm{AR}}(f)$, by searching for one harmonic frequency f_{hrm}, one sum interaction frequency f_{sum}, and one difference interaction frequency f_{diff}. Sets of frequencies are shown between curly brackets. Frequency is in min^{-1}. CC: chest compressions; PR: pulse rate; PSD: power spectral density.

$R_P = 0.05$ was used, because the AR model order P was selected such that the mean plus two standard deviations of the relative prediction error power was at most 5%. The spectral distribution observed in the PSDs determined $R_D = 0.5$.

2) PR Detection: To identify the PR, the relationship was determined between the frequencies of the peaks in $P_{\mathrm{AR}}(f)$. All spectral peaks were found by using the zero crossings from positive to negative in the derivative of $P_{\mathrm{AR}}(f)$. From all peaks found, a set of N_{pks} peaks $\{f_{\mathrm{pks}}\}$ was formed, where all frequencies were at least 18 min^{-1}, and deviated more than 5 min^{-1} from all compression rates $f_{cc,i}$ and harmonics $2 \cdot f_{cc,i}$ found in the window from which $P_{\mathrm{AR}}(f)$ was estimated.

Fig. 2 outlines the iterative algorithm that determined the relationship between the frequencies in $\{f_{\mathrm{pks}}\}$ to identify the PR. The frequency corresponding to the largest peak in $P_{\mathrm{AR}}(f)$ was not necessarily the PR, as measurements showed that the largest peak during compressions could correspond to an interaction frequency equal to the sum or the difference of the compression

rate and the PR. Therefore, the iterative algorithm determined the presence of interaction frequencies to identify the PR among the peaks.

The frequencies in $\{f_{\mathrm{pks}}\}$ were analyzed by iteratively creating subsets $\{f_i\}$ corresponding to the N_i largest peaks in the PSD. N_i was initialized at three and incremented by one until the PR had been identified or all N_{pks} frequencies had been analyzed. In each iteration, a set of PR candidates $\{f_{\mathrm{cnd}}\}$ was derived from $\{f_i\}$ by selecting the frequencies between 40 min^{-1} [9] and 250 min^{-1} [32]. For each PR candidate, three related frequencies were searched for in $\{f_i\}$ and collected in the set $\{f_{\mathrm{cnd,rel}}\}$: the harmonic $f_{\mathrm{hrm}} = 2 \cdot f_{cnd}$, the sum interaction frequency $f_{\mathrm{sum}} = f_{\mathrm{cnd}} + f_{cca}$, and the difference interaction frequency $f_{\mathrm{diff}} = |f_{\mathrm{cnd}} - f_{cca}|$. Interaction frequencies were considered only if the TTI signal contained compressions in the window from which $P_{\mathrm{AR}}(f)$ had been determined. Compression rate f_{cca} was the average of the rates $f_{cc,i}$ detected in this window. Frequencies were considered related if deviating at most Δf from the expected value. To identify the PR, a score was assigned to each candidate with related frequencies, by summing the corresponding peak values:

$$\mathrm{Score}(f_{\mathrm{cnd}}) = \sum_{f' \in \{f_{\mathrm{cnd}}, \{f_{\mathrm{cnd,rel}}\}\}} P_{\mathrm{AR}}(f'). \tag{24}$$

PR candidates without related frequencies had score zero. The scoring mechanism is related to Hinich's harmogram, where harmonics are added to detect a frequency [33]. PR candidates with a score equal to the strictly positive maximum of all scores were collected in the set $\{f_{\max}\}$. If there was one maximum with frequency $f_{\max}$, iterations stopped and a tentative identification $\mathrm{PR}_t[n]$ was obtained. If $f_{\max}$ had no associated harmonic f_{hrm}, but did have associated interaction frequencies f_{sum} and f_{diff}, with $P_{\mathrm{AR}}(f_{\mathrm{diff}})/P_{\mathrm{AR}}(f_{\max}) > k_1 > 1$ and $P_{\mathrm{AR}}(f_{\mathrm{diff}})/P_{\mathrm{AR}}(f_{\mathrm{sum}}) > k_2 > k_1$, with f_{diff} in $\{f_{\mathrm{cnd}}\}$, then $\mathrm{PR}_t[n] = f_{\mathrm{diff}}$. That is, based on the decreasing spectral amplitudes, f_{diff} was considered the PR, and both $f_{\max}$ and f_{sum} were considered sum interaction frequencies. However, if one of these conditions was not met, $\mathrm{PR}_t[n] = f_{max}$. Next, if the difference between the current and previous tentative identifications was at most Δf, the final identification was $\mathrm{PR}[n] = \mathrm{PR}_t[n]$. Otherwise, $\mathrm{PR}[n]$ could not be identified. If there was not one strictly positive maximum score, $\{f_{\max}\}$ was either empty, occurring when there were no related frequencies, or $\{f_{\max}\}$ contained multiple frequencies, occurring, e.g., when $\{f_i\}$ only contained the PR and one interaction frequency. In this case, the next iteration was performed. If $\{f_{\max}\}$ contained multiple frequencies when all N_{pks} peaks had been analyzed, it was determined whether $\{f_{\max}\}$ contained one frequency f' with minimum deviation $\epsilon = |\mathrm{PR}_t[n-1] - f'|$, with $\epsilon \leq \Delta f$. If so, $\mathrm{PR}[n] = \mathrm{PR}_t[n] = f'$, otherwise $\mathrm{PR}[n]$ and $\mathrm{PR}_t[n]$ could not be identified.

Parameters $k_1 = 3$ and $k_2 = 10$ were determined from the amplitude ratio observed between the associated peaks in the PSDs. Parameter $\Delta f = 15$ min^{-1} was determined from the frequency deviations observed in the PSDs.

3) Evaluation: The PR detection was evaluated in the 2-min cycle before the post-ROSC phase. Detection was considered correct if a PR was observed in the ABP, and if the detected PR was within 15 min^{-1} of the PR observed in the ABP spectrogram, and in the ABP signal during ventilations. The evaluation shows whether the detected PR can qualify the cardiac condition, but does not give the quantitative accuracy of the detected PR. From ABP signals identically high-pass filtered as PPG signals (see Section II-B) spectrograms were obtained using 10-s windows, translated by 1 s, and zero padded to 60 s.

G. Detection of Blood Volume Redistribution to the Periphery

When PR and compression rate coincide, the compression removal stage removes the spontaneous pulse, making the compression-free PPG signal unusable. However, when cardiogenic output resumed, a transient change in skin color could be observed, presumably caused by a redistribution of blood volume to the periphery and leading to a sudden decrease in the baseline of the PPG signal. We used the sudden decrease in baseline as an extra parameter to detect cardiogenic output, to accommodate for coinciding PR and compression rate.

The baseline of the PPG signal $\mathrm{ppg}_{\mathrm{bl\_d}}[n]$ was obtained by a cascade of three first-order Butterworth low-pass filters with an 0.5 Hz cutoff applied to the raw PPG signal $\mathrm{ppg}[n]$. Each filtering operation was followed by downsampling by a factor of two. Therefore, $\mathrm{ppg}_{\mathrm{bl\_d}}[n]$ was sampled at $f_{s\_d} = 31.25$ Hz.

To detect a sudden decrease in $\mathrm{ppg}_{\mathrm{bl\_d}}[n]$, a least squares regression line ρ_n was fitted in a window of N_{bl} (odd) samples:

$$\rho_n[n-m] = \beta_n \left[\frac{N_{\mathrm{bl}}-1}{2} - m\right] + \gamma_n,\ m = 0, \ldots, N_{\mathrm{bl}} - 1. \tag{25}$$

A sudden decrease in $\mathrm{ppg}_{\mathrm{bl\_d}}[n]$ was detected if the normalized rate of change

$$\Delta_{\mathrm{bl}}[n] = \beta_n (N_{\mathrm{bl}} - 1)/\gamma_n < \Delta_{\mathrm{BL}}, \tag{26}$$

with threshold $\Delta_{\mathrm{BL}} < 0$ [$(N_{\mathrm{bl}}$ samples$)^{-1}$]. Equation (26) was evaluated once per second. N_{bl} and Δ_{BL} were determined by inspecting the decrease in baseline for the animals with ROSC.

H. Indicator of Cardiogenic Output

To support ROSC assessment, the algorithm determined the state of an indicator of cardiogenic output, S_{ICO}:

1) $S_{\mathrm{ICO}} = 0$: No PR and no decrease in $\mathrm{ppg}_{\mathrm{bl\_d}}[n]$ were detected, i.e., "no detection" (red) in Fig. 1.
2) $S_{\mathrm{ICO}} = 1$: A decrease in $\mathrm{ppg}_{\mathrm{bl\_d}}[n]$ was detected, i.e., "Redistribution of blood volume to the periphery detected" (yellow) in Fig. 1.
3) $S_{\mathrm{ICO}} = 2$: A PR was detected in $P_{\mathrm{AR}}(f)$, i.e., "PR detected" (green) in Fig. 1.
4) $S_{\mathrm{ICO}} = 3$: A PR and a decrease in $\mathrm{ppg}_{\mathrm{bl\_d}}[n]$ were detected, i.e., states 1 and 2 held simultaneously (yellow and green in Fig. 1).

The state of indicator S_{ICO} was determined once per second.

I. Validation of the Indicator

To validate whether the indicator can support ROSC assessment, the indicator S_{ICO} was compared to the retrospective ROSC assessment of nine clinicians, who worked in the emergency department, operating room, intensive care unit or quick response team of the St. Elisabeth Hospital in Tilburg, The Netherlands. The clinicians were requested to assess at what time instant ROSC occurred in each experiment, so they would stop CPR. For this assessment, we provided the ECG, ABP, capnography, and carotid artery blood flow signals, as recorded over the entire experiment. We indicated upfront that the animals achieved ROSC. A ROSC annotation trace, indicating the number of clinicians having detected ROSC over time, was constructed from the provided time instants.

We used five parameters to quantify the performance of the indicator S_{ICO}. In the 2-min cycle before the post-ROSC phase, the time difference $\Delta T = T_I - T_C$ [s] was determined. We defined T_I as the time instant after which S_{ICO} contained no further episodes of $S_{\mathrm{ICO}} = 0$ which lasted 5 s or longer. We interpreted T_I as the start of consistent detection of cardiogenic output by S_{ICO}. We defined T_C as the median of the time instants at which the clinicians detected ROSC, to exclude early and late detections. Specificity and sensitivity were determined for S_{ICO} and the PR detection. Comparing the specificities and sensitivities shows the contribution of detecting decreases in $\mathrm{ppg}_{\mathrm{bl\_d}}[n]$ to S_{ICO}. The specificity SpICO was defined as the percentage of correct cardiac arrest detections by $S_{\mathrm{ICO}} = 0$ in the 20-min CPR period. The specificity SpPR was defined as the percentage of non-identified PRs in this period. The sensitivity SeICO was defined as the percentage of correct detections of cardiogenic output by $S_{\mathrm{ICO}} \neq 0$ between T_C and the start of the post-ROSC phase. The sensitivity SePR was defined as the percentage of identified PRs in this period.

III. Results

For consistency, the animal numbering from [20] has been adopted. Animals N1–N3 had no sustained ROSC. Animals R1–R9 had sustained ROSC. Animal N1 briefly had ROSC, but deteriorated to cardiac arrest again. For unambiguous annotation, the brief post-ROSC phase and the preceding 2-min cycle have been excluded from the data of animal N1.

To develop the algorithm, we used data from ten out of 16 animals. As in [20], four animals were excluded because the pulse oximeter probe interfered with the study PPG probe. This was resolved by increasing the distance between the probes. Further, animals R5 and R9 were excluded, because the snout was poorly perfused due to complications with the carotid arteries, and no TTI signal was recorded, respectively.

A. Determination of Compression Characteristics

Fig. 3 illustrates filtering of the measured TTI signal $Z[n]$ [see Fig. 3(a)] to obtain the fundamental compression component in $Z_f[n]$ [see Fig. 3(b)]. Local extremes are detected in $Z_f[n]$ (blue circles) to identify the onsets of individual compressions (red squares). Ventilation effects are partly suppressed in $Z_f[n]$.

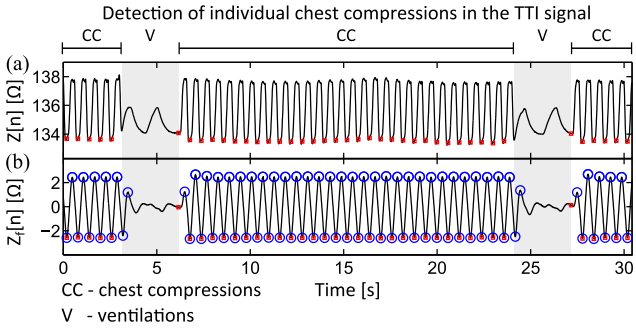

Fig. 3. (a) Measured TTI signal $Z[n]$. (b) Filtered TTI signal $Z_f[n]$ showing the fundamental compression component. Via the local extremes (blue circles) in $Z_f[n]$, the onsets of the individual compressions (red squares) are found. CC: chest compressions; TTI: transthoracic impedance; V: ventilations.

The compression rate $f_{cc,i}$ and phase $\phi_{cc}[n]$ [(5) and (7)], and the envelope function $A[n]$ were determined from the onsets. Compression rate $f_{cc,i}$ was found accurately, fluctuating slightly around 100 min^{-1} (see Table I). Only for animal N3 fluctuations were larger, due to a lower quality TTI signal.

B. Removal of the Compression Component

Fig. 4 illustrates removal of the compression component by a representative example. The defibrillation shock (dashed line) ends cardiac arrest, after which a spontaneous pulse appears. During arrest, the PPG signal $\mathrm{ppg}_{\mathrm{ac}}[n]$ in Fig. 4(a) shows the 30:2 CPR rhythm. When a spontaneous pulse appears, the complexity of $\mathrm{ppg}_{\mathrm{ac}}[n]$ increases during compressions. During arrest, the compression estimate $\mathrm{cmp}_{est}[n]$ in Fig. 4(b) is almost identical to the compressions in $\mathrm{ppg}_{\mathrm{ac}}[n]$. When a spontaneous pulse appears, $\mathrm{cmp}_{est}[n]$ changes shape. This is due to the harmonic of the PR at about 300 min^{-1}, which is close to a harmonic of the compression rate. Fig. 4(c) shows the compression-free PPG signal $\mathrm{ppg}_{\mathrm{cf}}[n]$ obtained by subtracting $\mathrm{cmp}_{est}[n]$ from $\mathrm{ppg}_{\mathrm{ac}}[n]$. The compression component is strongly reduced in $\mathrm{ppg}_{\mathrm{cf}}[n]$, although a decaying residual is present in $\mathrm{ppg}_{\mathrm{cf}}[n]$ at the start of a new compression sequence. During ventilations, the envelope function $A[n]$ forces $\mathrm{cmp}_{est}[n]$ to zero, leaving $\mathrm{ppg}_{\mathrm{ac}}[n]$ unaffected in $\mathrm{ppg}_{\mathrm{cf}}[n]$. During arrest, $\mathrm{ppg}_{\mathrm{cf}}[n]$ shows absence of a spontaneous pulse. During the first compression sequence after the shock, a spontaneous pulse appears in $\mathrm{ppg}_{\mathrm{cf}}[n]$. During compressions, the difference interaction frequency between the PR and the compression rate causes a low-frequency oscillation in $\mathrm{ppg}_{\mathrm{cf}}[n]$, which disappears when compressions stop.

The spectrograms in Fig. 5 illustrate the effective removal of the compressions. The PPG signal $\mathrm{ppg}_{\mathrm{ac}}[n]$ [see Fig. 5(a)] contains components at the compression rate and its harmonics during CPR, and components at the PR and its harmonics after successful defibrillation. The compression estimate $\mathrm{cmp}_{est}[n]$ [see Fig. 5(b)] mainly contains the compression frequency components, but can also contain frequency components related to the spontaneous pulse when these are close to the compression components (shortly after 33:00). The components at the compression rate and its harmonics are strongly reduced in the compression-free PPG signal $\mathrm{ppg}_{\mathrm{cf}}[n]$ [see Fig. 5(c)]. The

TABLE I
EVALUATION OF THE COMPRESSION RATE DETECTION, THE PR DETECTION, AND THE INDICATOR OF CARDIOGENIC OUTPUT

#	$f_{cc,i}$ [1/min]	PR		ΔT [s]	SpPR		SpICO		SePR		SeICO	
N1	100.0 ± 1.2	n.a.	n.a.	n.a.	100%	(1669/1669)	100%	(1664/1669)	n.a.	n.a.	n.a.	n.a.
N2	99.7 ± 1.2	n.a.	n.a.	n.a.	100%	(1821/1825)	99%	(1815/1825)	n.a.	n.a.	n.a.	n.a.
N3	100.0 ± 4.0	n.a.	n.a.	n.a.	95%	(1685/1766)	95%	(1676/1766)	n.a.	n.a.	n.a.	n.a.
R1	100.0 ± 0.9	77%	(49/64)	25	92%	(1125/1226)	88%	(1081/1226)	70%	(55/79)	72%	(57/79)
R2	99.8 ± 0.6	85%	(66/78)	46	91%	(1056/1161)	87%	(1006/1161)	74%	(74/100)	77%	(77/100)
R3	99.8 ± 0.6	56%	(9/16)	96	97%	(1271/1311)	96%	(1254/1311)	14%	(14/101)	22%	(22/101)
R4	99.9 ± 1.2	82%	(40/49)	69	97%	(1117/1151)	94%	(1083/1151)	52%	(49/94)	76%	(71/94)
R6	99.8 ± 1.3	86%	(65/76)	69	90%	(1080/1206)	89%	(1078/1206)	64%	(63/98)	64%	(63/98)
R7	100.0 ± 0.6	98%	(100/102)	-16	97%	(1169/1207)	95%	(1150/1207)	96%	(89/93)	96%	(89/93)
R8	99.9 ± 1.4	91%	(40/44)	3	99%	(1196/1214)	90%	(1098/1214)	75%	(44/59)	83%	(49/59)
Mean	99.9 ± 1.7	86%	(369/429)	42 ± 40	96%	(13189/13736)	94%	(12905/13736)	62%	(388/624)	69%	(428/624)

No ROSC: N1-3. ROSC: R1-4, R6-8. $f_{cc,i}$, mean ΔT in mean $\pm$ standard deviation. Correct detections over occurrences in parentheses. $f_{cc,i}$: compression rate; $\Delta T = T_I - T_C$, $T_{I,C}$: detection moment of ICO (I) and clinicians (C); SpPR: specificity PR detection; SpICO: specificity ICO; SePR: sensitivity PR detection; SeICO: sensitivity ICO; PR: pulse rate; ICO: indicator of cardiogenic output; n.a.: not applicable; ROSC: return of spontaneous circulation.

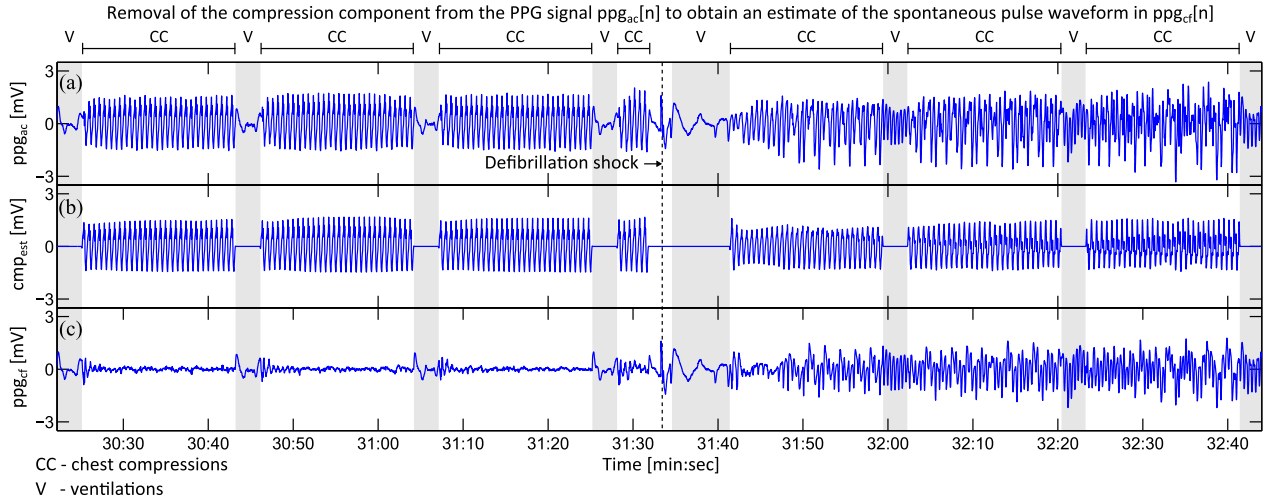

Fig. 4. (a) PPG signal $\mathrm{ppg_{ac}}[n]$. (b) Compression estimate $\mathrm{cmp}_{est}[n]$. (c) Compression-free PPG signal $\mathrm{ppg_{cf}}[n]$, obtained by subtracting $\mathrm{cmp}_{est}[n]$ from $\mathrm{ppg}_{ac}[n]$. Before the defibrillation shock (dashed line), a spontaneous pulse is absent in $\mathrm{ppg_{cf}}[n]$. During the first compression sequence after the shock, a spontaneous pulse appears in $\mathrm{ppg_{cf}}[n]$. This episode is part of the spectrograms in Fig. 5. CC: chest compressions; PPG: photoplethysmography; V: ventilations.

interaction frequencies, however, remain present in $\mathrm{ppg_{cf}}[n]$. The spectra of $\mathrm{ppg_{ac}}[n]$ and $\mathrm{ppg_{cf}}[n]$ contain interaction frequencies between the defibrillation shock and 32:30.

C. AR Model Order P

Fig. 6 shows the mean plus two standard deviations of the relative prediction error power as a function of AR model order P, which is at most 5% by selecting $P = 18$.

D. Spectral Analysis

Fig. 7 illustrates the spectral analysis. The PR detection algorithm (see Fig. 2) analyzes the peaks in the PSD $P_{\mathrm{AR}}(f)$ [see (19), Fig. 7(a)] to identify the PR, if a signal has been detected in the compression-free PPG signal $\mathrm{ppg_{cf\_d}}[n]$ [(20), SIG in Fig. 7(b)], with sufficient high-frequency content [(21), FD in Fig. 7(b)]. The SIG and FD conditions prevent analyzing most PSDs before the defibrillation shock (dashed line), when the animal is in cardiac arrest. When a PR has been identified [black dots in Fig. 7(c)], typically 3–4 peaks have been analyzed [purple dots in Fig. 7(c)] out of all peaks [blue circles in Fig. 7(c)]. During cardiac arrest, false PR detections occurred due to peaks deviating more than 5 min^{-1} from the compression rate or its second harmonic, as illustrated in Fig. 7(c). When the heart resumed cardiogenic output, 86% of the detected PRs was within 15 min^{-1} of the PRs observed in the ABP and, therefore, considered correct (PR in Table I). Comparing Fig. 7(c) to the ABP spectrogram in Fig. 7(d) shows 11 incorrect detections after the shock. Incorrect detections of the PR harmonic or a residual compression component at about 200 min^{-1} occur from 31:37 to 31:39, from 32:04 to 32:08, and at 32:16. Two more incorrect detections occur at 32:44 and 32:45. The remaining detected PRs can be recognized as PR in the ABP spectrogram, and are therefore considered correct. Between 32:09 and 32:23 no PR is detected, except for one false detection, when no relationships are found between the peaks.

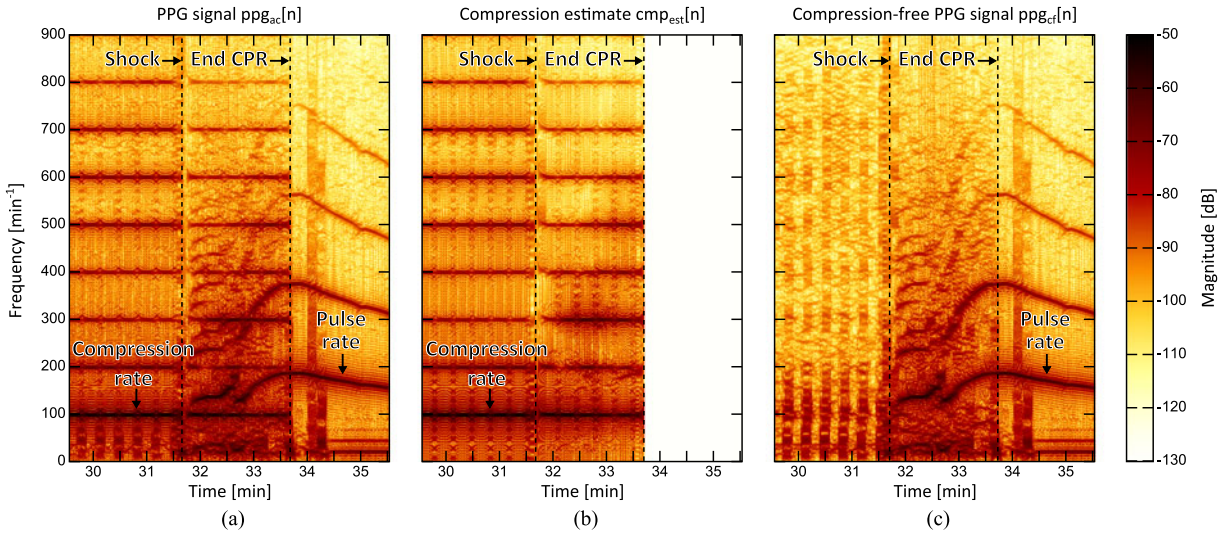

Fig. 5. Spectrograms of: (a) the PPG signal $\mathrm{ppg_{ac}}[n]$, (b) the compression estimate $\mathrm{cmp}_{est}[n]$, and (c) the compression-free PPG signal $\mathrm{ppg_{cf}}[n]$. The spectrograms show effective removal of the components at the compression rate and its harmonics in $\mathrm{ppg_{cf}}[n]$, achieved by subtracting $\mathrm{cmp}_{est}[n]$ from $\mathrm{ppg_{ac}}[n]$. After the defibrillation shock (first dashed line), a spontaneous pulse appears, which continues when CPR stops (second dashed line). The spectrograms have been obtained from 10-s windows, translated by 1 s, and zero padded to 60 s. They contain the episode of Fig. 4. CPR: cardiopulmonary resuscitation; PPG: photoplethysmography.

E. Detection of Blood Volume Redistribution to the Periphery

Fig. 8(a) shows that a pronounced decrease in the baseline of the PPG signal occurs, lasting at least 10 s, when cardiogenic output resumes in the animals with ROSC (thick lines). In contrast, this decrease is absent in animals without ROSC (thin lines). The decrease observed when cardiogenic output resumes can be detected by using $N_{\mathrm{bl}} = \lceil 5 \cdot f_{s\_d} \rceil = 157$ and $\Delta_{\mathrm{BL}} = -0.03$ [see Fig. 8(b)]. With these parameters, most fluctuations in baseline during cardiac arrest were not detected.

F. Validation of the Indicator

Fig. 9 presents the compression-free PPG signal $\mathrm{ppg_{cf\_d}}[n]$ of the animals with ROSC, the state of the indicator of cardiogenic output S_{ICO} and the ROSC annotation trace. The waveform and indicator show good agreement with the annotation. When clinicians detect ROSC, a spontaneous pulse is often present in $\mathrm{ppg_{cf\_d}}[n]$ and blood volume redistribution is detected. In animal R3, the spontaneous pulse occasionally has a PR of about 100 min^{-1}, and is therefore removed from $\mathrm{ppg_{cf\_d}}[n]$ by the compression removal stage, although $\mathrm{ppg_{cf\_d}}[n]$ then still shows presence of a spontaneous pulse during the ventilation periods. In animal R8 the spontaneous pulse appears clearly after the majority of clinicians detects ROSC. In animals R1, R4, and R8 blood volume redistribution has been detected before the first clinician detects ROSC.

For all animals in Fig. 9, the indicator detects cardiogenic output before the majority of the clinicians detects ROSC at time instant T_C, although consistent detection, on average, occurs 42 s after T_C (ΔT in Table I). By combining the detection of PR with decreases in PPG signal baseline in the indicator, the specificity decreased from SpPR $= 96\%$ to SpICO $= 94\%$, but the sensitivity increased from SePR $= 62\%$ to SeICO $= 69\%$ (see Table I). False detections of cardiogenic output by the indicator occurred in nine animals when CPR was started after cardiac arrest induction, when redistributing blood volume caused a decrease in the PPG signal baseline. False detections of cardiac arrest by the indicator were due to undetected PRs, caused by coinciding of the compression rate and the PR or their harmonics, $\mathrm{ppg_{cf\_d}}[n]$ not meeting the conditions on signal presence (see Section II-F1), or irregularity of $\mathrm{ppg_{cf\_d}}[n]$. However, when no PR was detected and the fundamental PR component had not been removed, $\mathrm{ppg_{cf\_d}}[n]$ could still show presence of a spontaneous pulse, and whether the spontaneous pulse had a regular or an irregular rhythm.

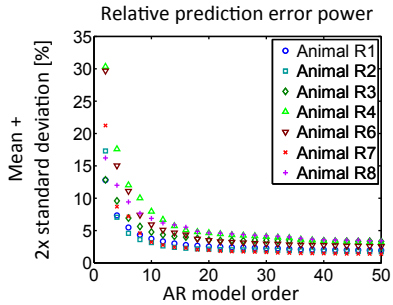

Fig. 6. Mean plus two standard deviations of the prediction error power relative to the compression-free PPG signal power as a function of AR model order for all animals with ROSC. AR: autoregressive; PPG: photoplethysmography; ROSC: return of spontaneous circulation.

IV. Discussion

Based on automated-CPR porcine data, we developed a PPG-based algorithm that detected cardiogenic output during chest compressions. A compression-free PPG signal was obtained by subtracting the compression component modeled by a harmonic series. The fundamental frequency of the series was the

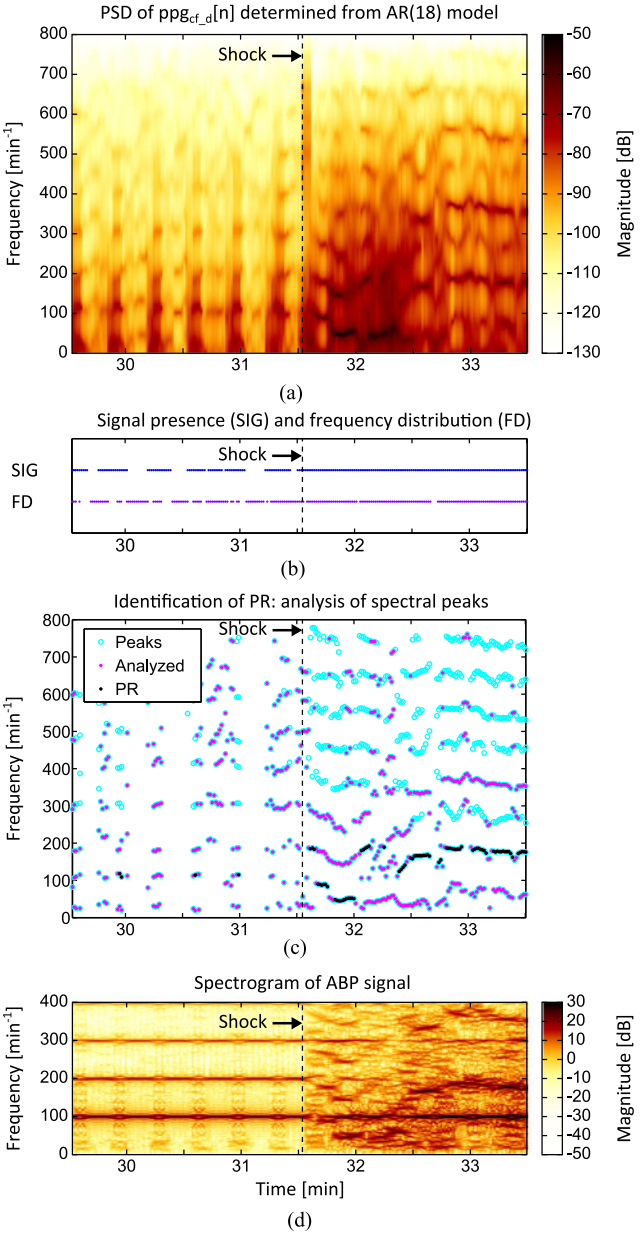

Fig. 7. (a) PSD $P_{\mathrm{AR}}(f)$ of the compression-free PPG signal $\mathrm{ppg}_{\mathrm{cf\_d}}[n]$, obtained from an order-18 AR-model. (b) Dots indicate detection of a signal in $\mathrm{ppg}_{\mathrm{cf\_d}}[n]$ [see SIG, (20)] having sufficient high-frequency content [FD, (21)]. If both conditions hold, PR detection is performed. (c) The PR detection algorithm analyzes a number (purple dots) of all peaks in the PSD (blue circles) to identify the PR (black dots). (d) Spectrogram of the ABP signal used to evaluate the PR detection. The dashed line indicates the defibrillation shock. ABP: arterial blood pressure; AR: autoregressive; PR: pulse rate; PPG: photoplethysmography; PSD: power spectral density.

compression rate derived from the TTI signal (see Fig. 3). During automated CPR, when compression rate and depth are controlled, removal of compressions was effective (see Figs. 4 and 5). Via an AR model, the PSD of the compression-free PPG signal $\mathrm{ppg}_{\mathrm{cf\_d}}[n]$ could be accurately obtained (see Fig. 6). The AR model allowed for detecting signal presence, and the PR could be identified in the PSD by searching for a harmonic of the PR and sum and difference interaction frequencies (see Fig. 7). When cardiogenic output resumed, the detected PR agreed for

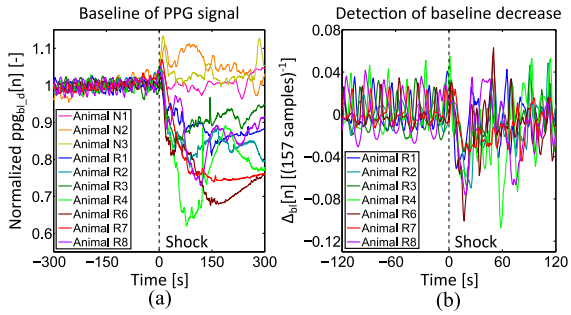

Fig. 8. (a) In animals with ROSC (thick line), the PPG signal baseline shows a pronounced decrease when cardiogenic output resumes. Without ROSC (thin line), such decrease is absent. The spikes in the traces of R3 and R4 are motion artifacts caused by changing the ventilator. Each baseline has been normalized by its mean over the 5 min preceding the shock. (b) Baseline decrease can be detected when $\Delta_{\mathrm{bl}}[n]$ decreases below -0.03 when using 5-s windows. All signals have been aligned with respect to the defibrillation shock at 0 s. PPG: photoplethysmography; ROSC: return of spontaneous circulation.

86% with the PR observed in the ABP (see Table I). Incorrect PR detections resulted from residual compression components, inadvertent removal of frequencies related to the spontaneous pulse, or irregularities in $\mathrm{ppg}_{\mathrm{cf\_d}}[n]$. The spontaneous pulse was removed from $\mathrm{ppg}_{\mathrm{cf\_d}}[n]$ when the PR was close to the compression rate [see Fig. 9(e)]. To accommodate for coinciding PR and compression rate, decreases in the baseline of the PPG signal were detected. Decreases in baseline occurred when cardiogenic output resumed (see Fig. 8), presumably caused by a redistribution of blood volume to the periphery. The indicator of cardiogenic output had a good specificity of 94% and a reasonable sensitivity of 69% (see Table I).

The compression-free PPG signal and the indicator can potentially support ROSC detection during compressions, as is illustrated by the good agreement with the ROSC annotation trace. The 94% specificity suggests that a PPG-based indicator can support detecting absence of cardiogenic output during compressions. In addition, Fig. 9 shows that the indicator detected presence of cardiogenic output before the majority of the clinicians detected ROSC, which suggests that a PPG-based indicator can also provide an early indication of ROSC or its development. Furthermore, Fig. 9 illustrates that the compression-free PPG signal can be more valuable to the clinician than the indicator alone. For example, the waveform can show presence of a spontaneous pulse when the PR cannot be determined, and allows for assessing the regularity of the spontaneous pulse during compressions. Therefore, this algorithm can support the clinician in deciding when it is appropriate to further assess a potential ROSC after a 2-min CPR cycle, although a single PPG signal does not provide quantitative information on blood pressure [19].

Detecting cardiogenic output during compressions can also support decision making in the CPR protocol. Information on cardiogenic output may support tailoring the duration of the compression sequence and medication choices to the clinical state of the patient [34]. Detecting absence of cardiogenic output during compressions may prevent interrupting compressions for futile and lengthy pulse checks [35]. Detecting presence of cardiogenic output during compressions may possibly guide

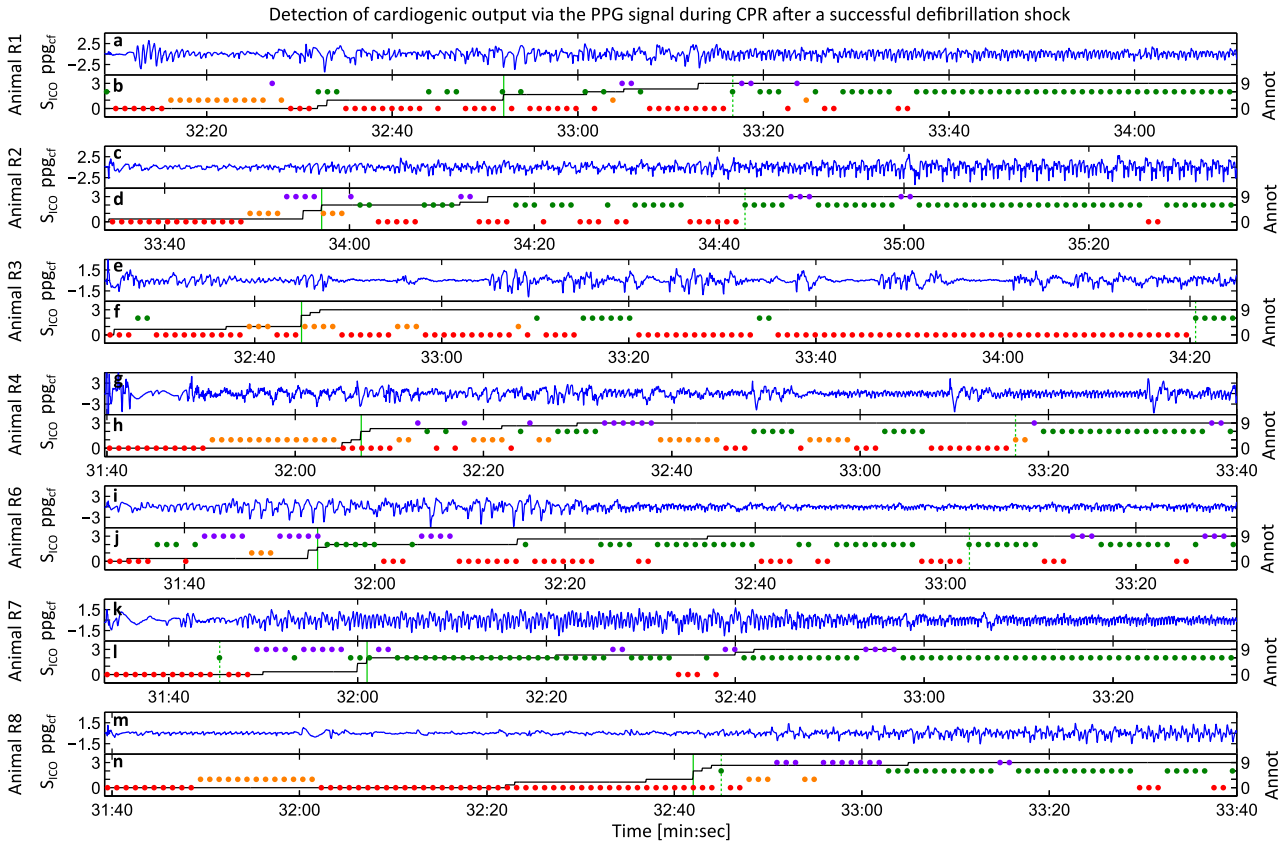

Fig. 9. The compression-free PPG signal $\mathrm{ppg}_{\mathrm{cf\_d}}[n]$ (a, c, e, g, i, k, m) combined with the indicator of cardiogenic output (b, d, f, h, j, l, n) can potentially support ROSC detection, as they show good agreement with the ROSC annotation trace (b, d, f ,h, j, l, n). The solid vertical green line marks T_C, the median of the instants that clinicians detected ROSC. The dashed vertical green line marks T_I, the moment after which interruptions in the indicator are shorter than 5 s. The traces start at the defibrillation shock. The first five oscillations in (a) are unfiltered compressions, due to incorrect detections in the TTI signal. CPR: cardiopulmonary resuscitation; PPG: photoplethysmography; PR: pulse rate; ROSC: return of spontaneous circulation; TTI: transthoracic impedance.

stopping compressions to reduce the risk of refibrillation, associated with continuing compressions on a beating heart [36]–[40]. Furthermore, detecting cardiogenic output during compressions may guide administration of vasopressors, which may have detrimental effects if administered when the heart has just resumed cardiogenic output [2].

The algorithm needs further improvement for clinical application, although 94% specificity is promising. Removal of the compression component was feasible in automated-CPR data. The varying compression rate and depth in manual CPR can require faster adaptation to changes in the PPG compression component and adaptive thresholds for TTI-based compression detection [21]–[23]. In the small preclinical dataset, parameter values were not extensively optimized. In a large clinical dataset, optimization can be performed and adaptive thresholds further investigated, to improve the algorithm performance as required for clinical application. The algorithm could operate in real time, despite that compression detection is delayed by two compressions, and AR and regression analysis operate on 5-s windows. Real-time operation can require an efficient implementation of AR analysis.

This study has limitations. First, we used porcine data obtained during automated CPR in a controlled laboratory environment. A clinical CPR study should show the ability of central and peripheral PPG signals to indicate cardiogenic output in humans during CPR [2], [41], and the suitability of the baseline of the PPG signal to support ROSC detection. Second, compressions and ventilations were alternated. The influence of ventilations during compressions on TTI-based compression detection should be further investigated [22].

V. Conclusion

Detecting cardiogenic output during chest compressions using a PPG-based algorithm is feasible in automated-CPR porcine data with a high specificity (94%). A compression-free PPG signal, containing an estimate of the spontaneous pulse waveform, can be obtained by subtracting the compression component modeled by a harmonic series, where the compression rate can be derived from the TTI signal. The PR can be detected in the AR spectrum of the compression-free PPG signal by identifying a harmonic and interaction frequencies. Resumed cardiogenic

output can also be detected from a decrease in the baseline of the PPG signal, presumably caused by a redistribution of blood volume to the periphery. ROSC detection can potentially be supported by combining the compression-free PPG signal with an indicator based on the detected PR and redistribution of blood volume.

ACKNOWLEDGMENT

The authors would like to thank Dr P. Woerlee, Ir P. Aelen, Ir I. Paulussen, and Dr S. Ordelman from Philips Research Eindhoven, and A. Venema MPA and P. Van Berkom MSc from St. Elisabeth Hospital Tilburg, for valuable discussions and conducting the experiments; Mr A. Hanssen, Ms W. Janssen-Kessel, and Mr M. School from the Central Animal Laboratory Nijmegen, and Prof. G.-J. Scheffer, Dr M. Kox, Ms F. Van de Pol, and K. Timmermans MSc from the Radboud University Nijmegen Medical Center for assistance during preparation and conduction of the experiments; and Mr B. Wassink from VDL ETG Research bv for technical assistance.

REFERENCES

[1] J. P. Nolan, "High-quality cardiopulmonary resuscitation," *Curr. Opin. Crit. Care*, vol. 20, no. 3, pp. 227–233, Jun. 2014.

[2] R. W. Neumar, C. W. Otto, M. S. Link, S. L. Kronick, M. Shuster, C. W. Callaway, P. J. Kudenchuk, J. P. Ornato, B. McNally, S. M. Silvers, R. S. Passman, R. D. White, E. P. Hess, W. Tang, D. Davis, E. Sinz, and L. J. Morrison, "Part 8: Adult advanced cardiovascular life support: 2010 American Heart Association guidelines for cardiopulmonary resuscitation and emergency cardiovascular care," *Circulation*, vol. 122, no. 18 Suppl 3, pp. S729–S767, Nov. 2010.

[3] C. D. Deakin, J. P. Nolan, J. Soar, K. Sunde, R. W. Koster, G. B. Smith, and G. D. Perkins, "European resuscitation council guidelines for resuscitation 2010 Section 4. Adult advanced life support," *Resuscitation*, vol. 81, no. 10, pp. 1305–1352, Oct. 2010.

[4] R. A. Berg, A. B. Sanders, K. B. Kern, R. W. Hilwig, J. W. Heidenreich, M. E. Porter, and G. A. Ewy, "Adverse hemodynamic effects of interrupting chest compressions for rescue breathing during cardiopulmonary resuscitation for ventricular fibrillation cardiac arrest," *Circulation*, vol. 104, no. 20, pp. 2465–2470, Nov. 2001.

[5] J. Christenson, D. Andrusiek, S. Everson-Stewart, P. Kudenchuk, D. Hostler, J. Powell, C. W. Callaway, D. Bishop, C. Vaillancourt, D. Davis, T. P. Aufderheide, A. Idris, J. A. Stouffer, I. Stiell, and R. Berg, "Chest compression fraction determines survival in patients with out-of-hospital ventricular fibrillation," *Circulation*, vol. 120, no. 13, pp. 1241–1247, Sep. 2009.

[6] B. Eberle, W. F. Dick, T. Schneider, G. Wisser, S. Doetsch, and I. Tzanova, "Checking the carotid pulse check: Diagnostic accuracy of first responders in patients with and without a pulse," *Resuscitation*, vol. 33, no. 2, pp. 107–116, Dec. 1996.

[7] J. Tibballs and P. Russell, "Reliability of pulse palpation by healthcare personnel to diagnose paediatric cardiac arrest," *Resuscitation*, vol. 80, no. 1, pp. 61–64, Jan. 2009.

[8] M. Pokorná, E. Nečas, J. Kratochvíl, R. Skipský, M. Andrlík, and O. Frank, "A sudden increase in partial pressure end-tidal carbon dioxide ($P_{ET}CO_2$) at the moment of return of spontaneous circulation," *J. Emerg. Med.*, vol. 38, no. 5, pp. 614–621, Jun. 2010.

[9] D. P. Davis, R. E. Sell, N. Wilkes, R. Sarno, R. D. Husa, E. M. Castillo, B. Lawrence, R. Fisher, C. Brainard, and J. V. Dunford, "Electrical and mechanical recovery of cardiac function following out-of-hospital cardiac arrest," *Resuscitation*, vol. 84, no. 1, pp. 25–30, Jan. 2013.

[10] N. A. Paradis, G. B. Martin, E. P. Rivers, M. G. Goetting, T. J. Appleton, M. Feingold, and R. M. Nowak, "Coronary perfusion pressure and the return of spontaneous circulation in human cardiopulmonary resuscitation," *J. Amer. Med. Assoc.*, vol. 263, no. 8, pp. 1106–1113, Feb. 1990.

[11] E. P. Rivers, J. Lozon, E. Enriquez, S. V. Havstad, G. B. Martin, C. A. Lewandowski, M. G. Goetting, J. A. Rosenberg, N. A. Paradis, and R. M. Nowak, "Simultaneous radial, femoral, and aortic arterial pressures during human cardiopulmonary resuscitation," *Crit. Care Med.*, vol. 21, no. 6, pp. 878–883, Jun. 1993.

[12] E. P. Rivers, G. B. Martin, H. Smithline, M. Y. Rady, C. H. Schultz, M. G. Goetting, T. J. Appleton, and R. M. Nowak, "The clinical implications of continuous central venous oxygen saturation during human CPR," *Ann. Emerg. Med.*, vol. 21, no. 9, pp. 1094–1101, Sep. 1992.

[13] H. Losert, M. Risdal, F. Sterz, J. Nysaether, K. Köhler, T. Eftestøl, C. Wandaller, H. Myklebust, T. Uray, S. O. Aase, and A. N. Laggner, "Thoracic-impedance changes measured via defibrillator pads can monitor signs of circulation," *Resuscitation*, vol. 73, no. 2, pp. 221–228, May 2007.

[14] M. Risdal, S. O. Aase, J. Kramer-Johansen, and T. Eftestøl, "Automatic identification of return of spontaneous circulation during cardiopulmonary resuscitation," *IEEE Trans. Biomed. Eng.*, vol. 55, no. 1, pp. 60–68, Jan. 2008.

[15] J. Ruiz, E. Alonso, E. Aramendi, J. Kramer-Johansen, T. Eftestøl, U. Ayala, and D. González-Otero, "Reliable extraction of the circulation component in the thoracic impedance measured by defibrillation pads," *Resuscitation*, vol. 84, no. 10, pp. 1345–1352, Oct. 2013.

[16] A. Kämäräinen, M. Sainio, K. T. Olkkola, H. Huhtala, J. Tenhunen, and S. Hoppu, "Quality controlled manual chest compressions and cerebral oxygenation during in-hospital cardiac arrest," *Resuscitation*, vol. 83, no. 1, pp. 138–142, Jan. 2012.

[17] S. Parnia, A. Nasir, C. Shah, R. Patel, A. Mani, and P. Richman, "A feasibility study evaluating the role of cerebral oximetry in predicting return of spontaneous circulation in cardiac arrest," *Resuscitation*, vol. 83, no. 8, pp. 982–985, Aug. 2012.

[18] J. Allen, "Photoplethysmography and its application in clinical physiological measurement," *Physiol. Meas.*, vol. 28, no. 3, pp. R1–R39, Mar. 2007.

[19] A. Reisner, P. A. Shaltis, D. McCombie, and H. H. Asada, "Utility of the photoplethysmogram in circulatory monitoring," *Anesthesiology*, vol. 108, no. 5, pp. 950–958, May 2008.

[20] R. W. C. G. R. Wijshoff, T. van der Sar, P. H. Peeters, R. Bezemer, P. Aelen, I. W. F. Paulussen, S. C. M. A. Ordelman, A. Venema, P. F. J. van Berkom, R. M. Aarts, P. H. Woerlee, G.-J. Scheffer, and G. J. Noordergraaf, "Detection of a spontaneous pulse in photoplethysmograms during automated cardiopulmonary resuscitation in a porcine model," *Resuscitation*, vol. 84, no. 11, pp. 1625–1632, Nov. 2013.

[21] E. Aramendi, U. Ayala, U. Irusta, E. Alonso, T. Eftestøl, and J. Kramer-Johansen, "Suppression of the cardiopulmonary resuscitation artefacts using the instantaneous chest compression rate extracted from the thoracic impedance," *Resuscitation*, vol. 83, no. 6, pp. 692–698, Jun. 2012.

[22] U. Ayala, T. Eftestøl, E. Alonso, U. Irusta, E. Aramendi, S. Wali, and J. Kramer-Johansen, "Automatic detection of chest compressions for the assessment of CPR-quality parameters," *Resuscitation*, vol. 85, no. 7, pp. 957–963, Jul. 2014.

[23] J. Ruiz, U. Irusta, S. Ruiz de Gauna, and T. Eftestøl, "Cardiopulmonary resuscitation artefact suppression using a Kalman filter and the frequency of chest compressions as the reference signal," *Resuscitation*, vol. 81, no. 9, pp. 1087–1094, Sep. 2010.

[24] U. Irusta, J. Ruiz, S. Ruiz de Gauna, T. Eftestøl, and J. Kramer-Johansen, "A least mean-square filter for the estimation of the cardiopulmonary resuscitation artifact based on the frequency of the compressions," *IEEE Trans. Biomed. Eng.*, vol. 56, no. 4, pp. 1052–1062, Apr. 2009.

[25] B. Widrow, J. R. Glover, J. M. McCool, J. Kaunitz, C. S. Williams, R. H. Hearn, J. R. Zeidler, E. Dong Jr., and R. C. Goodlin, "Adaptive noise cancelling: Principles and applications," *Proc. IEEE*, vol. 63, no. 12, pp. 105–112, Dec. 1975.

[26] Y. Xiao and Y. Tadokoro, "LMS-based notch filter for the estimation of sinusoidal signals in noise," *Signal Process.*, vol. 46, no. 2, pp. 223–231, Oct. 1995.

[27] S. M. Kay and S. L. Marple, "Spectrum analysis—A modern perspective," *Proc. IEEE*, vol. 69, no. 11, pp. 1380–1419, Nov. 1981.

[28] S. L. Marple Jr., "Corrections to "Spectrum analysis—A modern perspective," *Proc. IEEE*, vol. 70, no. 10, pp. 1238, Oct. 1982.

[29] D. A. Linkens, "Short-time-series spectral analysis of biomedical data," *Proc. IEE*, vol. 129, no. 9, pp. 663–672, Dec. 1982.

[30] S. G. Fleming and L. Tarassenko, "A comparison of signal processing techniques for the extraction of breathing rate from the photoplethysmogram," *Int. J. Biol. Med. Sci.*, vol. 1, no. 6, pp. 232–236, Oct. 2007.

[31] S. S. Haykin, Ed., *Nonlinear Methods of Spectral Analysis*. New York, NY, USA: Springer-Verlag, 1979.

[32] H. J. J. Wellens, K. I. Lie, and D. Durrer, "Further observations on ventricular tachycardia as studied by electrical stimulation of the heart: Chronic recurrent ventricular tachycardia and ventricular tachycardia during acute myocardial infarction," *Circulation*, vol. 49, no. 4, pp. 647–653, Apr. 1974.

[33] M. J. Hinich, "Detecting a hidden, periodic signal when its period is unknown," *IEEE Trans. Acoust., Speech, Signal Process.*, vol. ASSP-30, no. 5, pp. 747–750, Oct. 1982.

[34] T. Nordseth, D. P. Edelson, D. Bergum, T. M. Olasveengen, T. Eftestøl, R. Wiseth, J. T. Kvaløy, B. S. Abella, and E. Skogvoll, "Optimal loop duration during the provision of in-hospital advanced life support (ALS) to patients with an initial non-shockable rhythm," *Resuscitation*, vol. 85, no. 1, pp. 75–81, Jan. 2014.

[35] R. Wijshoff, T. van der Sar, R. Aarts, P. Woerlee, and G. Noordergraaf, "Potential of photoplethysmography to guide pulse checks during cardiopulmonary resuscitation: Observations in an animal study," *Resuscitation*, vol. 84, pp. S1–S7, Oct. 2013.

[36] J. Osorio, D. J. Dosdall, R. P. Robichaux, P. B. Tabereaux, and R. E. Ideker, "In a swine model, chest compressions cause ventricular capture and, by means of a long-short sequence, ventricular fibrillation," *Circulation., Arrhythmia Electrophysiol.*, vol. 1, no. 4, pp. 282–289, Oct. 2008.

[37] J. Osorio, D. J. Dosdall, P. B. Tabereaux, R. P. Robichaux, S. Stephens, J. D. Kerby, R. E. Stickney, S. Pogwizd, and R. E. Ideker, "Effect of chest compressions on ventricular activation," *Amer. J. Cardiol.*, vol. 109, no. 5, pp. 670–674, Mar. 2012.

[38] R. W. Koster, "Refibrillation during out-of-hospital arrest: A frequent event with clinical consequences," *Signa Vitae*, vol. 5, no. Suppl 1, pp. 66–68, 2010.

[39] J. Berdowski, J. G. P. Tijssen, and R. W. Koster, "Chest compressions cause recurrence of ventricular fibrillation after the first successful conversion by defibrillation in out-of-hospital cardiac arrest," *Circulation. Arrhythmia Electrophysiol.*, vol. 3, no. 1, pp. 72–78, Feb. 2010.

[40] A. Shiyovich, A. Gerovich, and A. Katz, "Recurrence of ventricular fibrillation after successful conversion, may be associated with immediate post-shock chest compressions: A case report," *Brit. J. Med. Med. Res.*, vol. 3, no. 3, pp. 722–726, Feb. 2013.

[41] R. D. Branson and P. D. Mannheimer, "Forehead oximetry in critically ill patients: The case for a new monitoring site," *Respir. Care Clin. North Amer.*, vol. 10, no. 3, pp. 359–367, Sep. 2004.

Authors' photographs and biographies not available at the time of publication.